# Relative Raman intensities of the folded modes in SiC polytypes

S. Nakashima, H. Katahama,* Y. Nakakura, and A. Mitsuishi
*Department of Applied Physics, Osaka University, Yamadaoka, Suita, Osaka 565, Japan*
(Received 8 July 1985)

A theoretical model, based on the bond-polarizability concept, is presented for the calculation of the Raman scattering intensities for crystals. The bonds in a unit cell are classified into groups in which the individual bond Raman polarizabilities are equivalent. The Raman polarizability of the crystals is expressed as the sum of the product of the bond Raman polarizability and the relative displacement of the end atoms linked by the bond. The theory is applied to the SiC polytypes. The calculated Raman intensity profiles reproduce qualitatively the observed Raman spectra of the folded modes which arise from TA- and TO-phonon branches along the $c$ direction.

## I. INTRODUCTION

Raman scattering has been widely used to obtain information about the vibrational properties of solids. The strength and nature of interatomic interactions are estimated from lattice-dynamical analyses of the phonon spectra. A considerable effort has been made in the prediction of the frequencies of Raman bands. However, very little attention has been paid to their relative Raman intensities, which should also provide information on the structure and the nature of interatomic interactions.

Recently the Raman spectra of folded modes have been measured by us[1] in various polytypes of layered crystals $CdI_2$ in which the phonons of the basic polytype (the $2H$ polytype) within the Brillouin zone and/or at the zone edge are reduced to the $\Gamma$ point by zone-folding effects. It has been found that the relative Raman intensities of these folded modes depend strongly on the stacking arrangement of polytypes. A model based on the interatomic polarizability (IAP) concept, which is an extension of the bond polarizability (BP) model, has explained qualitatively the Raman intensity profiles of $CdI_2$ polytypes. This fact demonstrates that the relative Raman intensity can be used to identify the polytype structures and also that the IAP model is applicable not only to layered crystals but also to three-dimensional polytypes such as SiC and ZnS. It is, however, to be noted that several additional assumptions are required in the IAP approach to describe the Raman intensity profiles of $CdI_2$ polytypes, because the interatomic interactions in $CdI_2$ are dominated mainly by ionic and van der Waals interactions.

In this work we provide a method whereby the Raman polarizability tensors of crystals are easily calculated by combining lattice-dynamical calculations with bond-Raman polarizability. This method is applied to SiC polytypes in order to examine the Raman intensity profile of the folded modes. The BP approach to the Raman intensity which was given for the first time by Wolkenstein,[2] and Eliashevich and Wolkenstein[3] and developed by Long[4] has been successfully applied to molecules. A few attempts have been made to interpret the Raman intensity profiles in Si,[5] crystals with diamond structure[6,7] and GaAs (Ref. 8) in terms of the bond polarizability. However, the comparison of the calculation and observation was possible only for the two-phonon spectra, because these crystals have only a single first-order Raman band (except TO-LO splitting).

We chose silicon carbide as a prototype crystal for study of the Raman intensities by means of the BP model, because a number of different polytypes of good quality, in which interatomic bonds are predominantly covalent, are available and many folded modes can be observed. Raman spectra of several SiC polytypes have been measured by Feldman *et al.*,[9,10] who have estimated the dispersion curves of the phonons propagating along the $c$ direction from the frequencies of the observed folded modes. The striking features of the spectra are as follows: First, relative Raman intensity of the folded modes depends strongly on the stacking sequence as in $CdI_2$. Second, there is a small splitting in the Raman bands which arises from the acoustic folded modes inside the Brillouin zone of the basic polytype ($3C$-SiC).

We have measured polarized Raman spectra of several SiC polytypes ($6H$, $8H$, $15R$, $21R$, and $27R$) at room temperature in the backscattering geometry to avoid the observation of oblique phonons. For these polytypes the relative Raman intensities have been calculated using a linear chain model and compared with the experiment. In general, good qualitative agreement between calculation and experiment is achieved. The experimental results are presented in Sec. II. In Sec. III, a theory for the calculation of the crystal Raman polarizabilities is presented and the expression for the Raman polarizability tensors is derived. Section IV gives the application of the theory to SiC polytypes. The relative Raman intensity of the folded modes is calculated using the bond-Raman polarizability together with the eigenvectors of the linear chain model. The experimental results for several polytypes are compared with the calculation. A brief discussion of the connection between the relative Raman intensities and lattice-dynamical calculation is given in Sec. V.

## II. EXPERIMENTAL RESULTS

SiC crystals used in this experiment were grown by the Acheson method. Thin crystal platelets having (0001)

 

TABLE I. Some of the simple SiC polytypes with three common notations.

| Ramsdell notation | *ABC* notation | *hk* notation | Space group | Atoms per unit cell |
|---|---|---|---|---|
| 3*C* | *ABC* | $k$ | $T_d^2$ | 2 |
| 2*H* | *AB* | $(h)_2$ | $C_{6v}^4$ | 4 |
| 4*H* | *ABAC* | $(hk)_2$ | $C_{6v}^4$ | 8 |
| 15*R* | *ABACBCACBABCBAC* | $(hkhkk)_3$ | $C_{3v}^5$ | 10 |
| 6*H* | *ABCACB* | $(hkk)_2$ | $C_{6v}^4$ | 12 |
| 21*R* | *ABCACBACABCBACBCABACB* | $(hkkhkkk)_3$ | $C_{3v}^5$ | 14 |
| 8*H* | *ABACBABC* | $(khkk)_2$ | $C_{6v}^4$ | 16 |

faces with a typical size of square millimeters and a few hundred micrometers thickness were examined. Polytypes were identified from the measured Raman frequencies. Several crystals were checked by x-ray analysis. The x-ray analysis showed that the 8*H* polytype used here contains 6*H*, partially. Table I shows the stacking sequences of several polytypes. In Table II we list the symmetry of normal modes. As shown in this table each of the folded modes arising from the phonons at midzone forms a doublet with the same symmetry. The $B_1$-type mode is Raman inactive.

Raman spectra were usually measured in backscattering geometry using the 4880-Å line of an $Ar^+$ laser. Figures 1(a)–1(d) and 2(a)–2(d) show Raman spectra of the polytypes 6*H*, 15*R*, 21*R*, and 8*H* which were measured in the backscattering configuration. The Raman bands observed in the frequency region below 260 $cm^{-1}$ correspond to folded transverse acoustic (TA) modes. The folded TO modes (*E*-type mode) are observed in the region from 750 to 810 $cm^{-1}$. The frequencies of the Raman bands agree well with results by Feldman *et al.*[9,10] within the experimental errors. For these polytypes the intensity of the Raman band lying originally at the Γ point (797 $cm^{-1}$ band) is relatively weak: A Raman band corresponding to the midzone phonon is more intense. As seen in Figs. 1 and 2, the Raman intensity profiles depend strongly on

TABLE II. Symmetry of phonon modes at the Γ point in several polytypes. $x=q/q_B$ is the reduced wave number of the phonon modes in the basic zone which is folded back to the Γ point by the zone folding along the *c* axis, where $q_B=\pi/c$. (The parentheses represent acoustic modes.)

| 2*H* phonon branch | $x=0$ | $x=1$ | | | |
|---|---|---|---|---|---|
| Planar acoustic | $(E_1)$ | $E_2$ | | | |
| Axial acoustic | $(A_1)$ | $B_1$ | | | |
| Planar optic | $E_1$ | $E_2$ | | | |
| Axial acoustic | $A_1$ | $B_1$ | | | |
| 15*R* | $x=0$ | $x=0.4$ | $x=0.8$ | | |
| Planar acoustic | $(E)$ | $2E$ | $2E$ | | |
| Axial acoustic | $(A)$ | $2A$ | $2A$ | | |
| Planar optic | $E$ | $2E$ | $2E$ | | |
| Axial optic | $A$ | $2A$ | $2A$ | | |
| 6*H* | $x=0$ | $x=0.33$ | $x=0.66$ | $x=1$ | |
| Planar acoustic | $(E_1)$ | $2E_2$ | $2E_1$ | $E_2$ | |
| Axial acoustic | $(A_1)$ | $2B_1$ | $2A_1$ | $B_1$ | |
| Planar optic | $E_1$ | $2E_2$ | $2E_1$ | $E_2$ | |
| Axial optic | $A_1$ | $2B_1$ | $2A_1$ | $B_1$ | |
| 21*R* | $x=0$ | $x=0.28$ | $x=0.57$ | $x=0.86$ | |
| Planar acoustic | $(E)$ | $2E$ | $2E$ | $2E$ | |
| Axial acoustic | $(A)$ | $2A$ | $2A$ | $2A$ | |
| Planar optic | $E$ | $2E$ | $2E$ | $2E$ | |
| Axial optic | $A$ | $2A$ | $2A$ | $2A$ | |
| 8*H* | $x=0$ | $x=0.25$ | $x=0.5$ | $x=0.75$ | $x=1$ |
| Planar acoustic | $(E_1)$ | $2E_2$ | $2E_1$ | $2E_2$ | $E_1$ |
| Axial acoustic | $(A_1)$ | $2B_1$ | $2A_1$ | $2B_1$ | $A_1$ |
| Planar optic | $E_1$ | $2E_2$ | $2E_1$ | $2E_2$ | $E_1$ |
| Axial optic | $A_1$ | $2B_1$ | $2A_2$ | $2B_1$ | $A_1$ |

the polytype. For folded modes of the TA branch, frequency splittings are observed when the modes correspond to the midzone phonon. Despite the fact that the symmetries of doublets are the same, the intensities of two partners are usually quite different. No splitting was observed in the doublets of the folded modes in the optical branches even at liquid-$N_2$ temperature. For the $8H$ polytype sample, the Raman bands corresponding to those of the $6H$ polytype are observed owing to the mixture of the $6H$ polytype.

Since the folded modes arise from the phonon modes at certain $q$ points in the basic zone, the measured frequencies of five polytypes are plotted in the form of dispersion curves in the basic zone in Fig. 3. The phonon mode at $q$ in the basic zone is denoted as the $q(x)$ mode hereafter, where $x=q/q_B$, $q_B=\pi/c$, and $c$ is the unit-cell length along the [111] direction of the $3C$ polytype (zinc blende).

We tried to observe the folded modes of the LA branch at the backscattering configuration $Z(X'Y'+X'X')\bar{Z}$, where $Z$ is parallel to the $c$ axis. Some folded modes of the $A$ branch (LO modes) are also Raman allowed at this scattering geometry. We could observe these Raman active modes, but their intensities were much weaker than those of the TA branch. Our measurements showed that the $q(0)$ mode was intense and other modes were very weak.

To probe $xz$ and $yz$ components of the Raman tensors, we measured Raman spectra using the backscattering

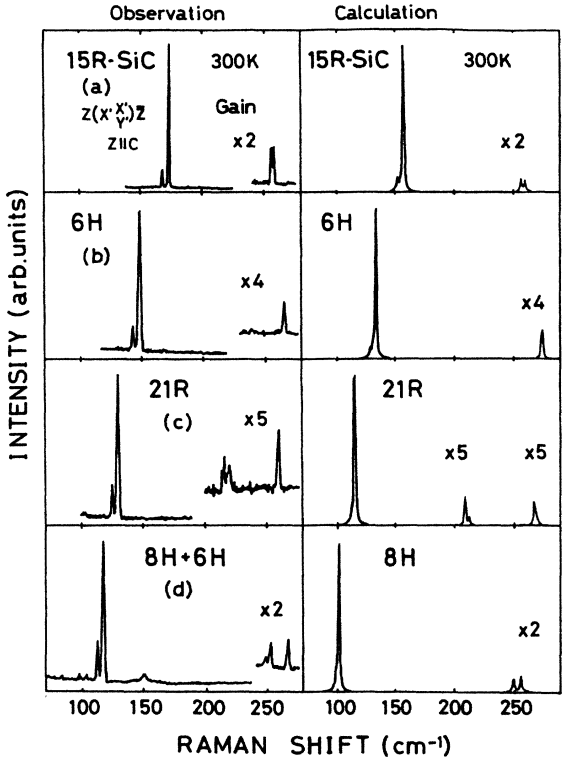


FIG. 1. Observed Raman spectra of the folded TA modes are compared with the calculation for four polytypes: (a) $15R$, (b) $6H$, (c) $21R$, and (d) $8H$. In the calculation, the bandwidth is chosen so as to fit the observed bands and a Bose-factor correction is made.

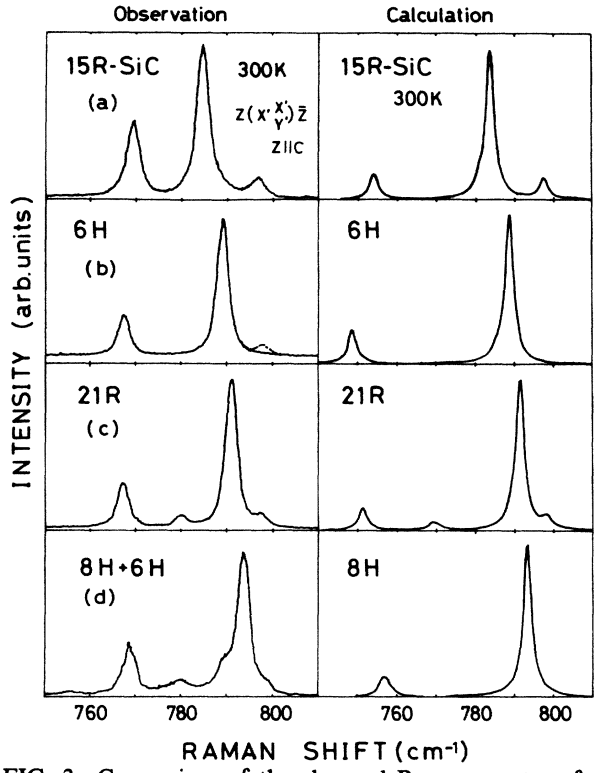


FIG. 2. Comparison of the observed Raman spectra of the folded TO modes with the calculation for four polytypes: (a) $15R$, (b) $6H$, (c) $21R$, and (d) $8H$. The dashed line shows the spectra measured with a $p$-polarized laser beam incident at an angle of $\sim 60°$.

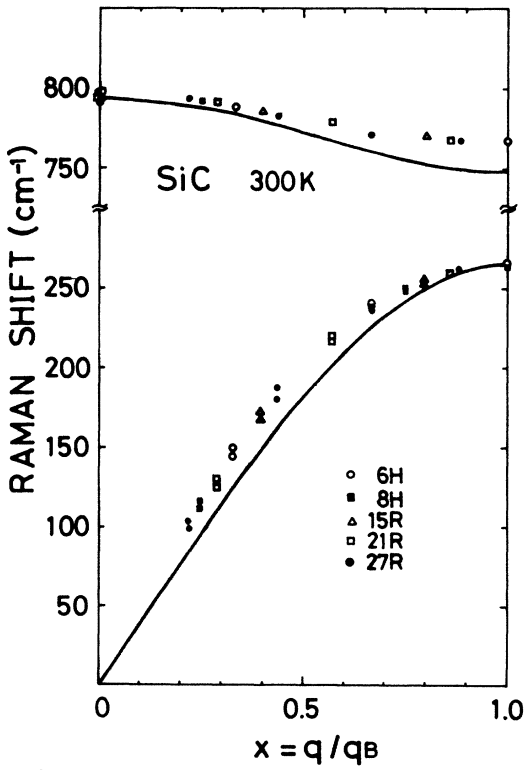


FIG. 3. Phonon dispersion curves in the basic zone using data from five polytypes. The solid lines show the linear-chain-model calculation. See text.

geometry, with a $p$-polarized laser beam incident at an angle of about 60°. The spectral features did not change except for the $q(0)$ optic mode at 797 $cm^{-1}$. As shown in Fig. 2(b) this band was not observed in the $s$ polarization for the $6H$ polytype, but was clearly observed in the $p$ polarization for which $xz$ or $yz$ components can be detected. For $8H$, $15R$, and $21R$ polytypes, the intensity of the $q(0)$ optic mode relative to other bands was also enhanced in the $p$ polarization.

## III. RAMAN POLARIZABILITY TENSORS

In the BP model[4,5,11] electrons of a crystal are divided into a number of groups which are assumed to be independent of one another. The bond polarizability is then additive with respect to groups of electrons

$$\underline{\alpha}=\sum_j \underline{\alpha}_j \ , \tag{1}$$

where $\underline{\alpha}_j$ is the polarizability of the $j$th group of electrons. The crystal polarizability $\underline{\alpha}$ takes the form

$$\underline{\alpha}=\sum_j \underline{\alpha}_j^B+\sum_j \underline{\alpha}_j^C \ ,$$

where labels $B$ and $C$ refer to bonds and cores, respectively. The $\underline{\alpha}_j^B$ and $\underline{\alpha}_j^C$ are symmetrical $3\times3$ tensors. For axially symmetric bonds we get

$$\underline{\alpha}_j^B=\begin{bmatrix}\alpha_\perp^j & 0 & 0\\ 0 & \alpha_\perp^j & 0\\ 0 & 0 & \alpha_{||}^j\end{bmatrix}, \quad \underline{\alpha}_j^C=\begin{bmatrix}\alpha_j^C & 0 & 0\\ 0 & \alpha_j^C & 0\\ 0 & 0 & \alpha_j^C\end{bmatrix}, \tag{2}$$

where $\alpha$ tensors are expressed in the principal-axis system of each bond and $\perp$ and $||$ refer to directions perpendicular and parallel to the bond, respectively. Transformation of this polarizability into that in the fixed crystal coordinate system is given by

$$\underline{\alpha}_j=\underline{R}_j^{-1}\underline{\alpha}_j^B\underline{R}_j \ , \tag{3}$$

where $\underline{R}_j$ is the rotation matrix. From the orthogonality relations for direction cosines, we get

$$[\alpha_j^B]_{\rho\sigma}=[\alpha_{||}^j-\alpha_\perp^j](j\rho)(j\sigma)+\alpha_\perp\delta_{\rho\sigma} \ , \tag{4}$$

where $(j\rho)$ is the direction cosine of the $j$th bond with the $\rho$th crystal axis. Assuming the bond polarizabilities to be additive, we obtain the tensor component of total polarizability of a unit cell in the crystal:

$$\alpha_{\rho\sigma}=\sum_{j=1}^{N_B}\{[\alpha_{||}^j-\alpha_\perp^j](j\rho)(j\sigma)+\alpha_\perp^j\delta_{\rho\sigma}\}+\sum_i^{N_C}\alpha_i \ , \tag{5}$$

where $N_B$ and $N_C$ are the number of chemical bonds and atomic cores in the unit cell, respectively.

The total tensor components $\alpha_{\rho\sigma}$ are a function of each bond length and also of bond orientation. Here we assume first that if a given bond is stretched, the components of that bond's polarizability tensor are altered but not those of any other bond,

$$\frac{\partial\alpha_{||}^j}{\partial r_l}=\frac{\partial\alpha_\perp^j}{\partial r_l}=0 \quad \text{for } l\neq j \ . \tag{6}$$

The second assumption is that the bond polarizability tensor does not change in magnitude with a change of the bond orientation, but the total tensor components are altered because of the direction cosine involved in a sum of Eq. (5), so that

$$\frac{\partial\alpha_{||}^j}{\partial(l\rho)}=\frac{\partial\alpha_\perp^j}{\partial(l\rho)}=0 \ . \tag{7}$$

The Raman scattering intensity of the $\lambda$th mode is related to the polarizability derivative with respect to the phonon normal coordinate $Q_\lambda$, i.e., the Raman polarizability tensor,

$$\alpha'_{\rho\sigma}(\lambda)=\frac{\partial\alpha_{\rho\sigma}}{\partial Q_\lambda} \ . \tag{8}$$

This quantity is expressed using the so-called intensity coordinate system which contains the $N_B$ bond stretchings and $3N_B$ changes of direction cosines, $2N_B$ of which are independent. The intensity coordinates are related to the Cartesian displacements $x$ by the $3N_B\times3m$ matrix $\underline{T}$,

$$\underline{I}=\underline{T}\,\underline{x}=\underline{T}\underline{M}^{-1}\underline{u} \ , \tag{9}$$

where $M_i^{1/2}x_i=u_i$, $\underline{M}=[(M_i)^{1/2}\delta_{ij}]$, and $M_i$ is the mass of the $i$th atom, and $m$ is the number of atoms in the unit cell. The matrix $\underline{T}$ is partitioned into submatrices, if we arrange the elements of the intensity coordinates related to respective bonds. Equation (9) is then written as

$$\underline{I}=\begin{bmatrix}\vdots\\ \Delta r_n\\ \Delta(nX)\\ \Delta(nY)\\ \vdots\end{bmatrix}=\begin{vmatrix}0 & T_{in}^s & 0 & T_{pn}^s & 0\end{vmatrix}\begin{bmatrix}i\\ x_i\\ y_i\\ z_i\\ \vdots\\ x_p\\ y_p\\ z_p\end{bmatrix} \ , \tag{10}$$

where $r_n$, $(nX)$, and $(nY)$ are elements of the intensity coordinates associated with the $n$th bond, and the subscripts $i$ and $p$ refer to the end atoms of the $n$th bond. The submatrices $T_{in}^s$ and $T_{pn}^s$ are $3\times3$ matrices expressed by

$$T_{in}^s=-T_{pn}^s=\begin{bmatrix}\frac{\partial r_n}{\partial x_i} & \frac{\partial r_n}{\partial y_i} & \frac{\partial r_n}{\partial z_i}\\ \frac{\partial(nX)}{\partial x_i} & \frac{\partial(nX)}{\partial y_i} & \frac{\partial(nX)}{\partial z_i}\\ \frac{\partial(nY)}{\partial x_i} & \frac{\partial(nY)}{\partial y_i} & \frac{\partial(nY)}{\partial z_i}\end{bmatrix} \ . \tag{11}$$

The phonon normal coordinates are related to the Cartesian displacement coordinates,

$$\underline{Q}=\underline{R}\,\underline{u}=\underline{R}\underline{M}\underline{X}=\underline{A}\underline{M}^2\underline{X} \ , \tag{12}$$

where $\underline{A}=\underline{R}\underline{M}^{-1}$ and $\underline{R}^{-1}=\underline{\tilde{R}}$. From Eqs. (9) and (12) we get

$$\underline{I}=\underline{T}\underline{\tilde{A}}\underline{Q} \ . \tag{13}$$

The matrix $\underline{A}$ is constructed from eigenvectors of the equations of motion. We then have

$$\frac{\partial \alpha_{\rho\sigma}}{\partial \underline{Q_\lambda}} = \frac{\partial \alpha_{\rho\sigma}}{\partial \underline{I_r}} \underline{T}\underline{\tilde{A}} , \tag{14}$$

where $\partial \underline{\alpha_{\rho\sigma}}/\partial Q_\lambda$ represents a column vector and $\partial \underline{\alpha_{\rho\sigma}}/\partial I_r$ is a row containing elements $\partial \alpha_{\rho\sigma}/\partial I_r$ which can be evaluated with the aid of Eq. (5). Nonvanishing elements of $\partial \underline{\alpha_{\rho\sigma}}/\partial I_r$ are given in the Appendix of Ref. 5.

We may write the row matrix $\partial \underline{\alpha_{\rho\sigma}}/\partial I_r$ as follows:

$$\frac{\partial \alpha_{\rho\sigma}}{\partial I_r} = \sum_n^{N_B} \left[ \ldots, 0, \frac{\partial [\alpha_n]_{\rho\sigma}}{\partial r_n}, \frac{\partial [\alpha_n]_{\rho\sigma}}{\partial (nX)} \frac{\partial [\alpha_n]_{\rho\sigma}}{\partial (nY)}, 0, \ldots, \right] . \tag{15}$$

Using Eqs. (11), (14), and (15), we have

$$\alpha'_{\rho\sigma}(\lambda) = \frac{\partial \alpha_{\rho\sigma}}{\partial Q_\lambda} = \sum_n^{N_B} \left[ \frac{\partial [\alpha_n]_{\rho\sigma}}{\partial x_i} (A_{\lambda x_i} - A_{\lambda x_p}) + \frac{\partial [\alpha_n]_{\rho\sigma}}{\partial y_i} (A_{\lambda y_i} - A_{\lambda y_p}) + \frac{\partial [\alpha_n]_{\rho\sigma}}{\partial z_i} (A_{\lambda z_i} - A_{\lambda z_p}) \right] , \tag{16}$$

where $i$ and $p$ refer to the end atoms of the $n$th bond and

$$\frac{\partial [\alpha_n]_{\rho\sigma}}{\partial x_i} = \frac{\partial [\alpha_n]_{\rho\sigma}}{\partial r_n} \frac{\partial r_n}{\partial x_i} + \frac{\partial [\alpha_n]_{\rho\sigma}}{\partial (nX)} \frac{\partial (nX)}{\partial x_i} + \frac{\partial [\alpha_n]_{\rho\sigma}}{\partial (nY)} \frac{\partial (nY)}{\partial x_i} . \tag{17}$$

A similar relation holds for $y_i$ and $z_i$. Since $A_{\lambda x_i}$ represents the displacement amplitude of the $i$th atom along the $x$ direction for the eigenfrequency $\omega_\lambda$, we see from Eq. (16) that the Raman tensors are dependent on the relative displacement between the neighboring atoms relevant to a bond.

In the framework of the BP model the first-order Raman spectra depend on the bond polarizabilities, their first derivatives with respect to the bond stretching coordinates, and the amplitudes of atomic vibrations (eigenvectors). Since the bond polarizabilities and their derivatives are not known *a priori*, we will start with the assumption that the bond polarizabilities and their derivatives are given and discuss only the relative intensities of different Raman bands.

Raman scattering efficiency is proportional to the square of the Raman polarizability tensor.[12] The Raman intensity for the $\lambda$th mode is given by

$$\overline{W}_\lambda = \frac{S}{W}(n_\omega + 1) \sum_{i,s} [\mathbf{e}_i \cdot \underline{\alpha}'(\lambda) \cdot \mathbf{e}_s]^2 , \tag{18}$$

where $S$ is a constant of proportionality which is independent of $\lambda$, $n_\omega$ is the Bose factor, and $\underline{\alpha}'(\lambda)$ is the Raman tensor whose component is given by Eq. (16). The summation in Eq. (18) is taken for degenerate modes.

## IV. APPLICATION TO SiC POLYTYPES

### A. Calculation of the Raman polarizability tensors

The structures of several SiC polytypes are shown in Fig. 4(a). The position of C is represented by Latin letters and Si atoms by Greek letters. The building units of all

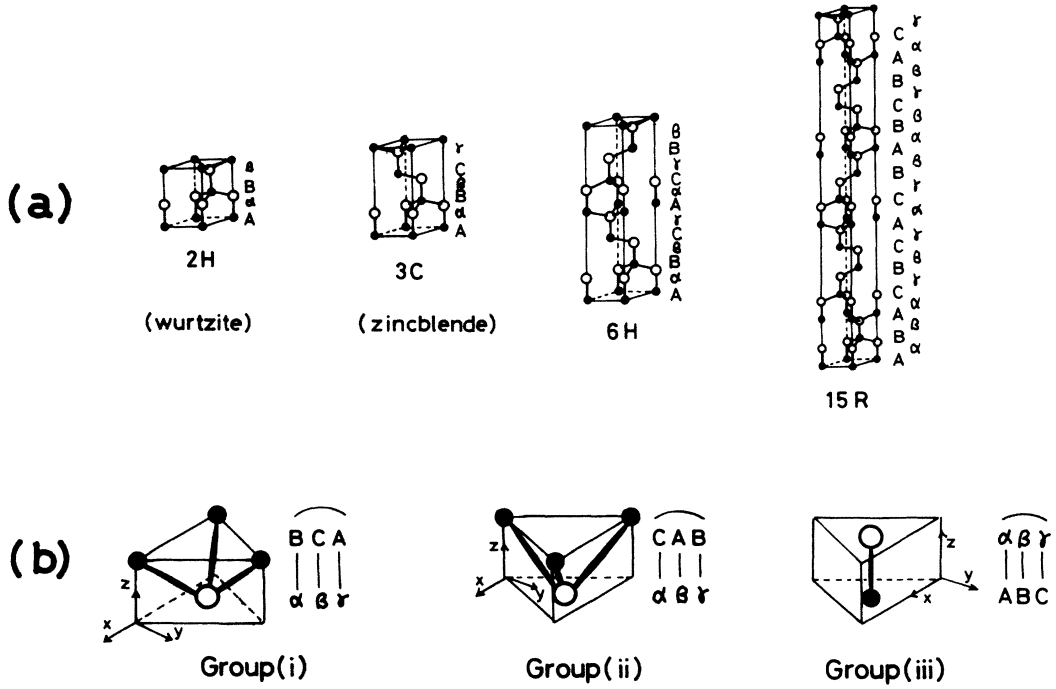


FIG. 4. (a) Several polytypes of SiC. Si and C atoms are shown by large open circles and small solid circles, respectively. (b) Bonding portions of Si-C are divided into three groups.

SiC polytypes are hexagonal double layers of Si-C. These are stacked together in such a way that each silicon atom is surrounded tetrahedrally by four carbon atoms and vice versa. For the configuration of the second neighbors, there are two types of configuration: a hexagonal configuration $h$ like that of atom $B$ in the sequence $ABA$ and a cubic configuration like that of atom $B$ in the sequence $ABC$. Spacings between Si-C planes along the $c$ axis which are linked by $A$-$\alpha$- and $A$-$\beta$-type bonds are $\frac{3}{4}c$ and $\frac{1}{4}c$, respectively. We assume, throughout this paper, that these spacings are independent of polytype structure. From the viewpoint of the contribution to the Raman polarizability, the bonds in the SiC polytypes are classified into three groups as shown in Fig. 4(b). The configurations of these bonding portions are (i) $\alpha B$, $\beta C$, and $\gamma A$, (ii) $\alpha C$, $\beta A$, and $\gamma B$, and (iii) $A\alpha$, $B\beta$, and $C\gamma$.

Using Eqs. (15) and (17), we have calculated the bond Raman polarizabilities $\partial[\alpha_n]_{\rho\sigma}/\partial x_i$, $\partial[\alpha_n]_{\rho\sigma}/\partial y_i$, and $\partial[\alpha_n]_{\rho\sigma}/\partial z_i$ for three types of the bonds, the result of which is shown in Table III, where for the groups (i) and (ii) the sum of the contributions from three bonds is considered. For the planar type displacements ($E$-type modes), each of the tensor components $\alpha'_{xx}$, $\alpha'_{yy}$, and $\alpha'_{xy}$ in Table III has the same magnitude but is different in its sign for groups (i) and (ii). The bonds in group (iii) do not contribute to these tensor components.

As described in Sec. II, our scattering geometry employed for the observation of the $E$-type modes allows only the components $\alpha'_{xx}(\lambda)$, $\alpha'_{xy}(\lambda)$, and $\alpha'_{yy}(\lambda)$. Since these three components are given by a parameter $c$ as shown in Table III, Eq. (16) can be rewritten as

$$\alpha'_{\rho\sigma}(E)=c\sum\pm(A^a_{Ex_j}-A^a_{Ex_{j+1}}), \tag{19}$$

for the $x$ polarization, where $A^a_{Ex_j}-A^a_{Ex_{j+1}}$ represents the relative displacement amplitude of neighboring atomic planes linked by the bonds in groups (i) and (ii), and the contributions from three bonds in groups (i) and (ii) are taken into account. The signs in Eq. (19) depend on the group to which the relevant bond belongs. From Eq. (19) we see that the calculation of the relative Raman intensities is now reduced to the determination of displacement amplitudes for respective atomic planes. An expression similar to Eq. (19) has been derived in Ref. 1 in order to explain the relative Raman intensities of the folded modes in $CdI_2$ polytypes.

The relative Raman intensities of the folded modes in the TA and TO branches can be calculated by use of Eqs. (18) and (19), if we determine the displacement amplitudes of the atomic planes from the equation of motion. It follows from Eq. (19) that the sign of all the tensor components $\alpha'_{\rho\sigma}(\lambda)$ is opposite for 180° out-of-phase displacements of the end atoms linked by a bond, e.g.,

$$\alpha'_{\rho\sigma}(\alpha\uparrow B\downarrow)=-\alpha'_{\rho\sigma}(\alpha\downarrow B\uparrow),$$

$$\alpha'_{\rho\sigma}(A\uparrow\alpha\downarrow)=-\alpha'_{\rho\sigma}(A\downarrow\alpha\uparrow),$$

TABLE III. Raman polarizability tensors of three groups of bonds for axial ($A$-type) and planar ($E$-type) vibrations. Symbols in parentheses indicate the direction of polarization of the phonons. $r$ is the bond distance.

(i)

$$\begin{array}{c} \\ \alpha\downarrow-B\uparrow \\ \beta\downarrow-C\uparrow \\ \gamma\downarrow-A\uparrow \end{array}\begin{array}{c} \\ \begin{pmatrix} a & 0 & 0 \\ 0 & a & 0 \\ 0 & 0 & b \end{pmatrix} \\ A(z) \end{array}\quad\begin{array}{c} \\ \begin{pmatrix} 0 & c & d \\ c & 0 & 0 \\ d & 0 & 0 \end{pmatrix} \\ E(x) \end{array}\quad\begin{array}{c} \\ \begin{pmatrix} c & 0 & 0 \\ 0 & -c & d \\ 0 & d & 0 \end{pmatrix} \\ E(y) \end{array}$$

(ii)

$$\begin{array}{c} \\ \alpha\downarrow-C\uparrow \\ \beta\downarrow-A\uparrow \\ \gamma\downarrow-B\uparrow \end{array}\begin{array}{c} \\ \begin{pmatrix} a & 0 & 0 \\ 0 & a & 0 \\ 0 & 0 & b \end{pmatrix} \\ A(z) \end{array}\quad\begin{array}{c} \\ \begin{pmatrix} 0 & -c & d \\ -c & 0 & 0 \\ d & 0 & 0 \end{pmatrix} \\ E(x) \end{array}\quad\begin{array}{c} \\ \begin{pmatrix} -c & 0 & 0 \\ 0 & c & d \\ 0 & d & 0 \end{pmatrix} \\ E(y) \end{array}$$

(iii)

$$\begin{array}{c} \\ A\downarrow-\alpha\uparrow \\ B\downarrow-\beta\uparrow \\ C\downarrow-\gamma\uparrow \end{array}\begin{array}{c} \\ \begin{pmatrix} e & 0 & 0 \\ 0 & e & 0 \\ 0 & 0 & f \end{pmatrix} \\ A(z) \end{array}\quad\begin{array}{c} \\ \begin{pmatrix} 0 & 0 & g \\ 0 & 0 & 0 \\ g & 0 & 0 \end{pmatrix} \\ E(x) \end{array}\quad\begin{array}{c} \\ \begin{pmatrix} 0 & 0 & 0 \\ 0 & 0 & g \\ 0 & g & 0 \end{pmatrix} \\ E(y) \end{array}$$

$$a=-\tfrac{4}{9}(\alpha'_{\parallel}-\alpha'_{\perp})-\frac{8}{9r}(\alpha_{\parallel}-\alpha_{\perp})-\alpha'_{\perp},\quad c=\frac{4\sqrt{2}}{9}(\alpha'_{\parallel}-\alpha'_{\perp})-\frac{8\sqrt{2}}{9r}(\alpha_{\parallel}-\alpha_{\perp}),$$

$$b=\tfrac{8}{9}(\alpha'_{\parallel}-\alpha'_{\perp})-\frac{16}{9r}(\alpha_{\parallel}-\alpha_{\perp})-\alpha'_{\parallel},\quad d=-\tfrac{4}{9}(\alpha'_{\parallel}-\alpha'_{\perp})-\frac{1}{9r}(\alpha_{\parallel}-\alpha_{\perp}),$$

$$e=\alpha'_{\perp},\quad f=\alpha'_{\parallel},\quad g=\frac{1}{r}(\alpha_{\parallel}-\alpha_{\perp}).$$

Thus, it is predicted that the tensor components $\alpha'_{xx}(\lambda)$, $\alpha'_{yy}(\lambda)$, and $\alpha'_{xy}(\lambda)$ of the bond in a hexagonal stacking are zero for the planar vibration such as $A\downarrow\alpha\uparrow B\downarrow\beta\uparrow A\downarrow$, if the amplitudes of the relative displacements, $\alpha\uparrow B\downarrow$ and $\beta\uparrow A\downarrow$, are equal.

Each diagonal tensor component of groups (i) and (ii) is equal for the axial vibrations ($A$-type modes). Accordingly, $\alpha'_{\rho\sigma}(\lambda)$ for the axial vibrations is expressed as

$$\alpha'_{\rho\rho}(\lambda)=\alpha^{(a)}_{\rho\rho}\sum_j (A^a_{\lambda z_j}-A^a_{\lambda z_{j+1}}) +\alpha^{(c)}_{\rho\rho}\sum_j (A^c_{\lambda z_j}-A^c_{\lambda z_{j+1}}) , \tag{20}$$

where

$$\alpha^{(a)}_{\rho\rho}=\begin{cases}=a & \text{for } \rho=x \text{ or } y,\\ =b & \text{for } \rho=z,\end{cases}$$

$$\alpha^{(c)}_{\rho\rho}=\begin{cases}=e & \text{for } \rho=x \text{ or } y,\\ =f & \text{for } \rho=z,\end{cases}$$

and $a$, $b$, $e$, and $f$ represent the bond-Raman polarizability components in Table III. The relative displacements along the $z$ direction, $A^a_{\lambda z_j}-A^a_{\lambda z_{j+1}}$, and $A^c_{\lambda z_j}-A^c_{\lambda z_{j+1}}$ refer to the neighboring atomic planes linked by the bonds in groups (i) and (ii) and group (iii), respectively. In Eq. (20) the contributions from three bonds in groups (i) and (ii) are taken into account.

We see that for the displacement pattern of the $q(x\neq 0)$ mode, there is always a set of relative displacement of the neighboring atoms which are 180° out of phase from each other. As a result, the summation in Eq. (20) becomes zero. Such cancellation also occurs for the Raman-tensor components $\alpha'_{xz}(\lambda)$ and $\alpha'_{yz}(\lambda)$ of the planar vibrations. This result means that except for $q(0)$ modes the Raman intensities of folded modes are negligibly small at any experimental geometries to probe diagonal components of the $A$-type modes and $xz$ and $yz$ components of the $E$-type modes.

For the $2H$ polytype the atomic displacement patterns of the $E_1$ and $E_2$ modes are described as $A\downarrow\alpha\uparrow B\downarrow\beta\uparrow$ and $A\downarrow\alpha\downarrow B\uparrow\beta\uparrow$, respectively. Raman tensors for the Raman active modes $A_1$, $E_1$, and $E_2$ are derived easily from Table III. The resulting Raman-tensor forms are identical with the expressions already derived.[12] The calculated results reflect the selection rule: All the tensor components of the Raman inactive modes $B$, which are the modes folded from the zone-edge phonons in the LA and LO branches, vanish.

We will extend the calculation described above to normal modes in polytype crystals. The next step to which we have to proceed is then to calculate the eigenvectors on which the Raman tensors depend substantially.

### B. Linear chain model

The phonons propagating along the $c$ direction are classified into the two groups: planar vibrations ($E$-type mode) and axial vibrations ($A$-type mode). For both types of vibrations atomic planes of C and Si perpendicular to the $c$ axis move as rigid units and hence a linear chain model is applicable.[13]

The equation of motion of the normal vibration can be written as

$$-M_j\ddot{X}_j=(K_{j,j+1}+K_{j,j-1})X_j-K_{j,j+1}X_{j+1}-K_{j,j-1}X_{j-1} =\sum_{n=\pm 1} D_{j,j+n}X_{j+n} , \tag{21}$$

where $K_{j,j\pm 1}$ is the nearest-neighbor plane force and $M_j$ is the mass of $j$th atomic plane. The force constant between the planes separated by $\frac{1}{4}c$ is taken as $F$, which is assumed to be equal for any polytype. The force constant between the planes separated by $\frac{3}{4}c$ has a small polytype dependence. Following Hodges[13] we write

$$K_{j,j+1}=K_{\text{cub}}+\Delta K_{j,j+1} . \tag{22}$$

If the double plane $A$-$\alpha$ occurs in a hexagonal environment, $\Delta K_{j,j+1}=K=K_{\text{hex}}-K_{\text{cub}}$ is not zero. Since the primitive unit cell of the $nH$ and $3nR$ polytypes contains $2n$ atomic planes, we get $2n$ equations of motion for the polytypes.

We look for the running wave solutions of the form

$$X_j=A_j\exp[i(\omega t-qx_j)] , \tag{23}$$

where $x=jc$ for C atoms and $x_{j'}=(j'+\frac{1}{4})c$ for Si atoms. Substitution of Eq. (23) in Eq. (21) leads to the following equations:

$$\sum_j [\delta_{ij}M_j\omega^2-D_{ij}(q)]A_j=0 . \tag{24}$$

This set of equations does not have trivial solutions if

$$|\,\delta_{ij}M_j\omega^2-D_{ij}(q)\,|=0 . \tag{25}$$

The frequencies of folded modes at the $\Gamma$ point are calculated numerically from Eq. (25) by taking force constants $F$, $K_{\text{cub}}$, and $\Delta K$ as fitting parameters. We have determined these force constants so that the experimental frequencies coincide with the calculated frequencies for the zone-center TO phonon and the folded mode corresponding to the zone-edge TA phonon in the basic zone and so that the calculated splitting of the $q(\frac{1}{3})$ modes of the TA branch fits the observed splitting in the $6H$ polytype. The fitting values of the force constants are $F=2.69\times 10^5$, $K=4.3\times 10^4$, and $\Delta K=5\times 10^3$ dyn/cm. The calculated eigenfrequencies are listed in Table IV. Letting $\Delta K=0$, we have calculated the dispersion curves in the basic zone, the result of which is shown in Fig. 3. The calculated frequencies of the TA branch are slightly smaller than the observed values. A slightly larger deviation from the experimental values, as much as 20 $\text{cm}^{-1}$, is found in the TO branch at around the zone edge. It is possible to fit the calculated values to the experimental result if we take into account the force constants between second neighbor planes. In this case, however, we are forced to use a unreal model where the second-neighbor forces are larger than the nearest-neighbor forces.

TABLE IV. Raman frequencies and relative Raman intensities measured at the $Z(X'X'+X'Y')\bar{Z}$ geometry are compared with calculated ones. The Raman intensity is normalized in such a way that the intensity of the strongest band of each branch is unity. Bose-factor correction is made for the calculated values.

| | | Frequency ($cm^{-1}$) | | | | Relative intensity ($I/I_{max}$) | | | |
|---|---|---|---|---|---|---|---|---|---|
| | | Optic | | Acoustic | | Optic | | Acoustic | |
| Polytype | $x=q/q_B$ | Expt. | Calc. | Expt. | Calc. | Expt. | Calc. | Expt. | Calc. |
| 15*R* | 0 | 798 | 797 | 0 | 0 | 0.12–0.095 | 0.14 | | |
| | 0.4 | 786 | 784 | 167 | 152 | 1.0 | 1.0 | 0.13–0.18 | 0.08 |
| | | | 781 | 173 | 157 | | 0.08 | 1.0 | 1.0 |
| | 0.8 | 770 | 754 | 255 | 258 | 0.49 | 0.06 | 0.12 | 0.038 |
| | | | 753 | 256 | 261 | | 0.12 | 0.13 | 0.034 |
| 6*H* | 0 | 798 | 0 | 0 | 0 | 0 | 0 | | |
| | 0.33 | 789 | 786 | 140 | 129 | 1.0 | 1.0 | 0.17–0.15 | 0.04 |
| | | | 785 | 150 | 133 | | 0.04 | 1.0 | 1.0 |
| | 0.66 | | 763 | | 230 | 0 | 0 | 0 | 0 |
| | | | 761 | | 238 | | 0 | ~0.014 | 0 |
| | 1.0 | 768 | 748 | 266 | 276 | 0.3–0.28 | 0.23 | 0.047–0.06 | 0.05 |
| 21*R* | 0 | 797 | 798 | 0 | 0 | 0.045 | 0.07 | | |
| | 0.28 | 792 | 791 | 126 | 112 | 1.0 | 1.0 | 0.26–0.23 | 0.035 |
| | | | 788 | 131 | 115 | | 0.035 | 1.0 | 1.0 |
| | 0.57 | 779 | 770 | 217 | 208 | 0.065 | 0.013 | 0.05–0.04 | 0.04 |
| | | | 769 | 220 | 212 | | 0.048 | 0.04–0.01 | 0.011 |
| | 0.86 | 768 | 752 | | 268 | 0.30 | 0.04 | 0.083 | 0.03 |
| | | | 751 | | 269 | | 0.12 | 0.055 | 0.015 |
| 8*H* | 0 | 796 | 798 | 0 | 0 | 0 | 0 | | |
| | 0.25 | 792 | 793 | 112 | 99 | 1.0 | 1.0 | 0.3 | 0.03 |
| | | | 791 | 117 | 101 | | 0.015 | 1.0 | 1.0 |
| | 0.5 | | 777 | | 186 | | 0 | 0 | 0 |
| | | | 774 | | 191 | | 0 | 0 | 0 |
| | 0.75 | | 758 | 248 | 249 | 0 | 0.07 | 0.076 | 0.042 |
| | | | 756 | 251 | 256 | | 0.09 | 0.19 | 0.05 |
| | 1.0 | 767 | 749 | 266 | 277 | 0.35[a] | 0 | 0.23[a] | 0 |

[a]Due to the 6*H*-polytype component.

### C. A comparison with the observed spectra

The relative amplitudes of displacements $A_{\lambda j}$ are obtained for respective eigenfrequencies $\omega_\lambda$. Using Eqs. (18) and (19) and calculated $A^q_{\lambda j}$, we calculate the relative Raman intensity of the *E*-type folded modes. The result is described in Table IV. In Figs. 1 and 2 we compare the calculation with the observed Raman profiles for four polytypes. The intensity of the Raman bands is normalized in such a way that the intensity of the strongest band in each branch of the polytypes is unity. As seen in Figs. 1 and 2, the calculation reproduces well the observed intensity profiles except for some modes. Our calculation predicts that the Raman intensities are zero for the $q(\frac{2}{3})$ modes of the TO and TA branches in the 6*H* polytype and for the $q(\frac{1}{2})$ and $q(1)$ modes in the 8*H* polytype. This prediction is consistent with the result of group-theory analysis. Although the $q(0)$ mode of the TO branch is also expected to be missing for both polytypes, a very weak shoulder is observed at about 797 $cm^{-1}$ for the 8*H* polytype. For the 8*H* and 21*R* polytypes a remarkable discrepancy is seen for the low-frequency partner of the $q(\frac{1}{4})$ and $q(\frac{2}{7})$ modes, respectively, in the TA branch: The calculated intensity ratio of the low-frequency partner to the high-frequency one is one order of magnitude smaller than the observed ratio. Regardless of the quantitative discrepancy found in some folded modes, general features of the Raman spectra for the planar-type folded modes are interpreted satisfactorily by the present model. It is to be noted that in this model we do not need to determine the four parameters $\alpha_{||}$, $\alpha_\perp$, $\alpha'_{||}$, and $\alpha'_\perp$ as we are concerned with the relative Raman intensity of the folded modes for each phonon branch.

## V. DISCUSSION AND CONCLUSION

Our model calculation reveals that the Raman-tensor components of the axial vibration (*A*-type mode) vanish for all the folded modes except the $q(0)$ modes. However, Raman active folded modes of the LA branch have been observed, though their intensity is very weak. The reasons for this discrepancy would be that (1) the presence of unequal spacings[14] between the Si and C planes along the *c* axis in higher polytypes causes incomplete cancellations in the Raman polarizability, and (2) the electro-optic effect, which is not considered in the present model, contributes

to the intensity of longitudinal phonons.[12]

As mentioned in Sec. IV, the disagreement between the calculated and experimental frequencies of the folded modes can be removed if the second-neighbor plane forces are included in the linear chain model. However, the Raman intensity calculated by this model gives rise to a large discrepancy between the experimental results and calculation, especially for the doublets of the folded modes. Another shortcoming in the use of the linear chain model is that although the theory explains the relative Raman intensity of the folded modes in each branch, the calculated intensity ratio of the folded TO modes to folded TA modes is larger than the observed ratio. This is due to the fact that the linear chain model yields a rather large force constant for the bond between the Si and C planes separated by $\frac{1}{4}c$. More refined models including long-range forces will be needed to reproduce both relative Raman intensities and frequencies of the folded modes, simultaneously. Since Raman scattering intensity is more sensitive than eigenfrequencies to the eigenvectors of relevant phonon modes, the analysis of the Raman intensities will provide a rigorous check on the validity of the lattice-dynamical model employed. With some modifications of the approximations in the model, our model based on the bond-polarizability concept is applicable not only to covalent crystals but also to partially ionic crystals.

From the viewpoint of application, the measurement of Raman frequencies and intensities is a useful technique for identifying the structure of the SiC polytypes and determining the amount of the mixture in composites of different polytypes.

## ACKNOWLEDGMENTS

The authors are grateful to Dr. Z. Inoue of the Institute of Inorganic Materials for the x-ray analyses of the polytype used in this experiment. We wish to thank Professor R. F. Wallis for his careful reading of the manuscript.

---

*Present address: Central Research Laboratory, Sumitomo Metal Industries, Ltd., 1-3 Nishinagasu-Hondori, Amagasaki, Hyogo 660, Japan.

[1]S. Nakashima, H. Katahama, Y. Nakakura, A. Mitsuishi, and B. Pal osz, Phys. Rev. B **31**, 6531 (1985).

[2]M. Wolkenstein, C. R. (Dokl.) Acad. Sci. URSS **30**, 791 (1941).

[3]M. Eliashevich and M. Wolkenstein, J. Phys. (Moscow) **9**, 101 (1945); **9**, 326 (1945).

[4]D. A. Long, Proc. R. Soc. London Ser. A **217**, 203 (1953).

[5]R. Tubino and L. Piseri, Phys. Rev. B **11**, 5145 (1975).

[6]S. Go, H. Bilz, and M. Cardona, Phys. Rev. Lett. **34**, 580 (1975).

[7]A. A. Maradudin and E. Burstein, Phys. Rev. **164**, 1081 (1967).

[8]S. Go, H. Bilz, and M. Cardona, *Proceedings of the Third International Conference on Light Scattering in Solids, Campinas, Brazil (1975),* edited by M. Balkanski, R. C. C. Leite, and S. P. S. Porto (Wiley, New York, 1975), p. 377.

[9]D. W. Feldman, J. H. Parker, Jr., W. J. Choyke, and L. Patrick, Phys. Rev. **170**, 698 (1968).

[10]D. W. Feldman, J. H. Parker, Jr., W. J. Choyke, and L. Patrick, Phys. Rev. **173**, 787 (1968).

[11]R. E. Hester, *Raman Spectroscopy,* edited by H. A. Szymanski (Plenum, New York, 1967), p. 101.

[12]R. Loudon, Adv. Phys. **13**, 423 (1964).

[13]C. H. Hodges, Phys. Rev. **187**, 994 (1969).

[14]A. H. Gomes de Mesquita, Acta Crystallogr. **23**, 610 (1967).